

PET of Hypoxia with ^{89}Zr -Labeled cG250-F(ab')₂ in Head and Neck Tumors

Bianca A.W. Hoeben¹, Johannes H.A.M. Kaanders¹, Gerben M. Franssen², Esther G.C. Troost¹, Paul F.J.W. Rijken¹, Egbert Oosterwijk³, Guus A.M.S. van Dongen⁴, Wim J.G. Oyen², Otto C. Boerman², and Johan Bussink¹

¹Department of Radiation Oncology, Radboud University Nijmegen Medical Centre, Nijmegen, The Netherlands; ²Department of Nuclear Medicine, Radboud University Nijmegen Medical Centre, Nijmegen, The Netherlands; ³Department of Urology, Radboud University Nijmegen Medical Centre, Nijmegen, The Netherlands; and ⁴Department of Otolaryngology/Head and Neck Surgery, VU University Medical Center, Amsterdam, The Netherlands

Hypoxic tumor cells are resistant to radiotherapy and various chemotherapeutic agents. The pretherapeutic assessment of intratumoral hypoxia may allow selection of patients for intensified treatment regimens. Carbonic anhydrase IX (CAIX) is an endogenous hypoxia-related protein involved in pH regulation and is upregulated in many tumor types. Radionuclide imaging using a monoclonal antibody against CAIX, such as cG250, may allow noninvasive PET of hypoxia in these tumor types. The aims of this study were to investigate whether ^{89}Zr -labeled cG250-F(ab')₂ allowed visualization of tumor hypoxia using small-animal PET and whether the tracer showed spatial correlation to the microscopic distribution of CAIX-expressing cells in a human head and neck xenograft tumor model. **Methods:** Athymic mice with subcutaneous human head and neck carcinoma xenografts (SCCNij3) were imaged with small-animal PET after injection of ^{89}Zr -cG250-F(ab')₂. PET images were parameterized in terms of standardized uptake values (SUVs). After injection with the nitroimidazole hypoxia marker pimonidazole and the perfusion marker Hoechst 33342, the animals were sacrificed, tumors excised, and CAIX- and pimonidazole-marked hypoxia and blood perfusion were analyzed immunohistochemically. ^{89}Zr -cG250-F(ab')₂ tumor uptake was analyzed by ex vivo activity counting and by autoradiography of tumor sections. **Results:** As early as 4 h after administration, accumulation of ^{89}Zr -cG250-F(ab')₂ in the tumor had occurred and tumors were clearly visualized by PET, with reduced uptake by 24 h after injection. Pixel-by-pixel analysis showed a significant positive spatial correlation between CAIX expression and ^{89}Zr -cG250-F(ab')₂ localization ($r = 0.57\text{--}0.74$; $P < 0.0001$). Also, significant correlations were found between pimonidazole staining intensity and ^{89}Zr -cG250-F(ab')₂ activity concentration, although less strong ($r = 0.46\text{--}0.68$; $P < 0.0001$). Tumor maximum SUV correlated significantly with tumor uptake determined ex vivo ($r = 0.93$; $P = 0.0067$), as did fractions of CAIX and pimonidazole in tumor sections ($r = 0.75$; $P = 0.03$ and $r = 0.78$; $P = 0.02$, respectively). **Conclusion:** ^{89}Zr -labeled cG250-F(ab')₂ small-animal PET showed rapid accumulation in a head and neck xenograft tumor model with good correlation to CAIX expression on a microscopic level.

Key Words: small-animal PET; cG250-F(ab')₂; head and neck carcinoma; hypoxia; CAIX

J Nucl Med 2010; 51:1076–1083
DOI: 10.2967/jnumed.109.073189

Tumor hypoxia is associated with poor prognosis in many tumor types because of progression toward a more malignant phenotype, with increased metastatic potential and increased resistance to treatment (1).

Hypoxia can stabilize and increase the levels of the transcription factor hypoxia-inducible factor-1 α (HIF-1 α), which has various downstream targets involved in adapting to hypoxia through, for example, angiogenesis, maintenance of pH balance, and anaerobic glycolysis (2). One of the downstream targets of HIF-1 α is carbonic anhydrase IX (CAIX), which plays an important role in pH homeostasis by catalyzing the reversible hydration of carbon dioxide to carbonic acid (3,4). CAIX is involved in maintaining a stable intracellular pH with acidification of the extracellular microenvironment (5). Upregulation occurs at pO₂ levels below 20 mm Hg, and CAIX has been validated as an intrinsic hypoxia-related cell marker (4,6). CAIX is attractive for the in vivo assessment of hypoxia, because of its relatively high expression on the cell surface and, unlike HIF-1 α , its long half-life in hypoxic tissues (4). Among normal tissues, CAIX is restricted to low-level expression in the gastric mucosa, bile ducts, and small intestine.

Various tools to assess and quantify CAIX expression have been developed, including G250 IgG, a monoclonal antibody against CAIX (7,8). A chimeric version was developed as a tumor marker of clear cell renal cell carcinoma, in which CAIX is upregulated in all cells because of the inactivation of the von Hippel–Lindau tumor suppressor protein (9,10). Because CAIX expression in most other tumor types is generally correlated with hypoxia, we hypothesized that radiolabeled cG250 could be used as a noninvasive imaging tool to visualize hypoxic regions in

Received Nov. 26, 2009; revision accepted Mar. 4, 2010.

For correspondence or reprints contact: Bianca A.W. Hoeben, Department of Radiation Oncology, Radboud University Nijmegen Medical Centre, P.O. Box 9101, 6500 HB Nijmegen, The Netherlands.

E-mail: b.hoeben@rther.umcn.nl

COPYRIGHT © 2010 by the Society of Nuclear Medicine, Inc.

tumors and also to select patients for hypoxia-targeting or -modifying treatment combined with radiotherapy (11). Another approach to specifically target hypoxic cells is by applying intensity-modulated radiotherapy with dose escalation to hypoxic tumor volumes detected by imaging (12).

Antibody fragments tend to show better tumor penetration than intact IgG (13). An earlier study with cG250 IgG showed no apparent correlation between ^{111}In -cG250 uptake and fractions of tumor sections stained with pimonidazole (an exogenous bioreductive hypoxia marker) or CAIX in head and neck tumor models (14). Enzymatic degradation of intact IgG monoclonal antibodies with pepsin results in formation of $\text{F}(\text{ab}')_2$ fragments with a smaller molecular size. Compared with intact IgG, $\text{F}(\text{ab}')_2$ fragments have a much shorter residence time in blood and normal tissues (15,16). In the present study, we assessed ^{89}Zr -cG250- $\text{F}(\text{ab}')_2$ as a PET marker of hypoxia. We investigated the spatial relationship between intratumoral distribution of ^{89}Zr -labeled cG250- $\text{F}(\text{ab}')_2$ as determined by autoradiography and immunohistochemical detection of CAIX and pimonidazole in a head and neck xenograft tumor model. In this model, we also investigated whether ^{89}Zr -cG250- $\text{F}(\text{ab}')_2$ accumulation could be used for the imaging of tumor hypoxia using small-animal PET.

MATERIALS AND METHODS

Xenograft Tumor Model

Eighteen BALB/c *nu/nu* mice with subcutaneously xenografted SCCNij3 head and neck squamous cell carcinomas were used. Eight mice were used to qualitatively determine the intratumoral distribution of radiolabeled cG250 using autoradiography. In the experiment with radiolabeled cG250- $\text{F}(\text{ab}')_2$, 10 mice were used for tumor activity counting *ex vivo*, and 8 of these were used for imaging with small-animal PET, immunohistochemistry, and autoradiography. One-cubic-millimeter tumor pieces were transplanted subcutaneously in the right hind leg of 6- to 8-wk-old mice. Experiments started at an average tumor diameter of 6–8 mm. Animals were kept in a specific pathogen-free unit in accordance with institutional guidelines. The Animal Welfare Committee of the Radboud University Nijmegen Medical Centre approved all experiments.

cG250- $\text{F}(\text{ab}')_2$ Fragments

cG250- $\text{F}(\text{ab}')_2$ fragments (molecular weight, ~ 100 kDa) were produced from intact IgG monoclonal antibodies cG250 (molecular weight, ~ 150 kDa) (Wilex AG). In a study by Brouwers et al., the affinity of ^{125}I -cG250- $\text{F}(\text{ab}')_2$ was $2.6 \times 10^9 \text{ M}^{-1}$, and the affinity of parental ^{125}I -cG250-IgG was $2.3 \times 10^9 \text{ M}^{-1}$ in the same assay (17). Five milligrams of cG250 were digested with 0.125 mg of pepsin (Boehringer) in 0.1 M citrate buffer, pH 3.8. After 6 h at 37°C , digestion was stopped by adding 0.25 mL of 1.0 M Tris. Nondigested IgG was removed by affinity chromatography using an Econo-Pac protein A column (Bio-Rad Laboratories) with binding buffer (3 M NaCl, 1.5 M Glycine), pH 8.9. The $\text{F}(\text{ab}')_2$ -containing fragments were buffer-changed to NaCl 0.9% by ultrafiltration using a Centricon YM-10 (Millipore) and stored at 4°C . Sodium dodecyl sulfate–polyacrylamide gel electrophore-

sis analysis showed no apparent residual IgG or formation of Fab' fragments during digestion (Supplemental Fig. 1; supplemental materials are available online only at <http://jnm.snmjournals.org>).

Conjugation, Radiolabeling, and Quality Control

The diethylenetriaminepentaacetic acid–cG250-IgG conjugate was radiolabeled with ^{111}In and injected intravenously in 8 mice with subcutaneous SCCNij3 tumors, as described previously (14). For imaging with cG250- $\text{F}(\text{ab}')_2$, the radionuclide ^{89}Zr was chosen because of its residualizing traits and half-life, which match the *in vivo* pharmacokinetics of $\text{F}(\text{ab}')_2$. ^{89}Zr has a 78-h half-life and emits positrons with a mean energy of 0.4 MeV (yield, 0.23). To allow ^{89}Zr labeling, cG250- $\text{F}(\text{ab}')_2$ was conjugated with the chelate desferrioxamine B mesylate (Desferal; Novartis) via an amide linkage. *N*-suc-desferrioxamine-cG250- $\text{F}(\text{ab}')_2$ was labeled as described by Verel et al. (18). The antibody (2.5 mg) and *N*-succinylferrioxamine tetrafluorophenol (66 nmol; VU University Medical Center) were conjugated in Na_2CO_3 (pH 9.7) at room temperature for 30 min. After conjugation, the reaction mixture was adjusted to pH 4.4 with 0.25 M H_2SO_4 , and the iron was removed from the chelator using an excess of ethylenediaminetetraacetic acid at 35°C . After 30 min, the *N*-suc-desferrioxamine-cG250- $\text{F}(\text{ab}')_2$ conjugate was purified using a PD-10 column (GE Healthcare) and eluted with 0.9% NaCl/gentisic acid (5 mg/mL, pH 5).

The *N*-suc-desferrioxamine-cG250- $\text{F}(\text{ab}')_2$ (0.5 mg) was radiolabeled with 360 MBq of ^{89}Zr (IBA Molecular) in a total volume of 2 mL. The ^{89}Zr oxalate was adjusted to pH 4.1 using 2 M Na_2CO_3 . After 3 min of mixing, the solution was adjusted to pH 6.9 with 0.5 M *N*-(2-hydroxyethyl)piperazine-*N'*-(2-ethanesulfonic acid), and *N*-suc-desferrioxamine-cG250- $\text{F}(\text{ab}')_2$ (0.5 mg) was added and incubated for 60 min at 37°C . The labeling efficiency (60%) was determined by instant thin-layer chromatography.

The ^{89}Zr -labeled *N*-suc-desferrioxamine-cG250- $\text{F}(\text{ab}')_2$ preparation, hereafter called ^{89}Zr -cG250- $\text{F}(\text{ab}')_2$, was purified by gel filtration on a PD-10 column, and radiochemical purity ($>95\%$) was checked by instant thin-layer chromatography. ^{89}Zr -cG250- $\text{F}(\text{ab}')_2$ (21 μg of cG250- $\text{F}(\text{ab}')_2$, 0.41 MBq/ μg) was diluted in 0.9% NaCl/gentisic acid (5 mg/mL, pH 5) to a volume of 200 μL per mouse. The immunoreactive fraction of the radiolabeled cG250- $\text{F}(\text{ab}')_2$ preparations was determined using freshly trypsinized SK-RC-52 cells as described previously, with minor modifications (19). Briefly, ^{89}Zr -cG250- $\text{F}(\text{ab}')_2$ (12,000 disintegrations per minute [200 Bq]) was incubated with increasing concentrations of SK-RC-52 tumor cells in 0.5 mL of binding buffer (RPMI 1640 medium containing 0.5% bovine serum albumin). A duplicate of the lowest cell concentration was incubated in the presence of an excess of unlabeled cG250- $\text{F}(\text{ab}')_2$ to correct for nonspecific binding. After incubation for 1 h at 37°C , cells were washed with 500 μL of binding buffer, and the cell-bound activity was determined using a γ -counter (1480 Wallac Wizard 3"; Perkin Elmer). The inverse of the tumor cell-bound fraction was plotted against the inverse of the cell concentration, and the immunoreactive fraction (74%) was calculated from the *y*-axis intercept.

Small-Animal PET and Biodistribution

Ten mice were injected intravenously with 200 μL of a ^{89}Zr -cG250- $\text{F}(\text{ab}')_2$ solution (42.5 MBq/mL). Syringes were measured in a dose calibrator before and after injection, indicating that mice received 6.85 ± 0.55 MBq of ^{89}Zr -cG250- $\text{F}(\text{ab}')_2$. Images were

acquired at 4 ($n = 4$) and 24 h ($n = 4$) after injection with an Inveon small-animal PET scanner (Siemens Preclinical Solutions). Thirty minutes before imaging, mice were injected intraperitoneally with 80 mg of pimonidazole per kilogram (gift from James A. Raleigh, Department of Radiation Oncology, University of North Carolina). Animals were imaged in pairs while anesthetized using isoflurane. Tumors on the right hind legs were positioned in the center of the field of view. At 4 h after injection, a 30-min emission scan was acquired in 4 animals. For attenuation correction, 7-min transmission scans were recorded after emission scans, using the built-in ^{57}Co source of 131 MBq (energy window, 120–125 keV). From the 4 animals imaged at 24 h after injection, 45-min emission scans were acquired, followed by 7-min transmission scans. One transmission scan at 24 h after injection could not be acquired.

The perfusion marker Hoechst 33342 (15 mg/kg; Sigma) was injected intravenously 1 min before the animal was killed. The tumors and selected normal tissues (muscle and blood) were harvested, weighed, and counted in a γ -well counter. Tumors were cut in half; one half of the tumor was immediately snap-frozen in liquid nitrogen for autoradiography and immunohistochemical staining purposes. Radioactivity uptake in the other half of the tumor was calculated as percentage of the injected dose per gram of tissue (%ID/g). To correct for radioactive decay, injection standards were counted simultaneously. Radioactive uptake of ^{89}Zr -cG250-F(ab')₂ in tumors was compared with fractions of tumor area positively stained for CAIX (fCAIX) and pimonidazole (fPIMO) in tumor sections.

PET Image Analysis

List-mode data were acquired using the default energy and coincidence timing windows of 350–650 keV and 3.4 ns, respectively, and histogrammed into a 3-dimensional sinogram (20). Data were reconstructed for analysis using ordered-subset expectation maximization in 3 dimensions (2 iterations), followed by maximum a posteriori (18 iterations) reconstruction. Maximum a posteriori reconstructions were performed with $\beta = 0.05$ and were optimized for uniform resolution. The transaxial pixel size was 0.431 mm, section thickness 0.796 mm, and image matrix size $256 \times 256 \times 161$.

PET images were analyzed using Siemens Inveon Research Workplace software (version 1.3; Siemens Preclinical Solutions). Regions of interest (ROIs) were manually placed around the tumor and left kidney. ROIs of a single volume were drawn over the liver and hind leg muscle. Quantification of tracer uptake in the ROIs of the attenuation-corrected slices was obtained by calculating the maximum standardized uptake values (SUV_{max}). One PET scan at 24 h after injection could not be attenuation-corrected, and SUV_{max} values from this scan (2 mice) were disregarded.

Autoradiography

Frozen central tumor sections (5 μm thick) were mounted on poly-L-lysine-coated slides and fixed in acetone before autoradiography, allowing adequate autoradiography with optimal immunohistochemical staining quality. Slides were exposed to a Fujifilm BAS cassette 2025 overnight (Fuji Photo Film). Phospholuminescence plates were scanned using a Fuji BAS-1800 II bioimaging analyzer at a pixel size of $50 \times 50 \mu\text{m}$. Images were processed with Aida Image Analyzer software (Raytest). The same tumor sections were used for immunohistochemical staining and analysis.

Immunohistochemical Staining

Slides were scanned for the fluorescent Hoechst 33342 signal before staining for CAIX, pimonidazole, and blood vessels. Between consecutive steps of the staining process, sections were rinsed 3 times for 5 min in phosphate-buffered saline (Klinipath). Primary antibodies were diluted in primary antibody diluent (GeneTex Inc.) and secondary antibodies in phosphate-buffered saline. Sections were incubated overnight (4°C) with biotinylated mouse anti-CAIX (G250) antibody (mouse-anti-CAIX-Biotin), diluted 1:150. Then sections were incubated with mouse anti-biotinCy3 (Jackson Immunoresearch Laboratories), diluted 1:400 (45 min, 37°C), followed by incubation with Fab fragment donkey antimouse IgG, diluted 1:50, and rabbit antipimonidazole, diluted 1:1,000 for 45 min at room temperature. Next, sections were incubated with 9F1 (rat monoclonal antibody against mouse endothelium; Radboud University Nijmegen Medical Centre), undiluted for 30 min at room temperature, followed by incubation with chicken antirat-Alexa647 1:200 (Molecular Probes) and donkey antirabbit-Alexa488 1:400 (Molecular Probes) for 30 min at 37°C. Finally, all nuclei were stained using Hoechst, diluted 1:3,000, for 5 min. Sections were mounted in Fluorostab (ICN).

Immunohistochemistry Image Acquisition and Analysis

Tumor sections were analyzed using a digital image analysis system, as described previously (21). After whole-tissue sections had been scanned, gray-scale images (pixel size, $2.59 \times 2.59 \mu\text{m}$) for vessels, perfusion, CAIX, and pimonidazole were obtained and subsequently converted into binary images. Thresholds for segmentation of the fluorescent signals were interactively set above the background staining for each individual marker. Binary images were used to calculate fCAIX and fPIMO relative to the total tumor area. Areas of necrosis, determined using hematoxylin- and eosin-stained neighboring tumor sections, were excluded from analysis.

Spatial Colocalization Analysis

The autoradiography and immunohistochemistry images were coregistered using ImageJ software (free JAVA-based image-processing package) and its Turbo-Registration plug-in package (22). The pixel size of the immunohistochemistry images was rescaled to match that of the autoradiography images ($50 \times 50 \mu\text{m}$). After alignment, all images were rescaled to a pixel size of $200 \times 200 \mu\text{m}$, corresponding to the estimated accuracy of image coregistration. Before rescaling to $200 \times 200 \mu\text{m}$ pixels, a mean smoothing of the pixel signal with an appropriate radius was applied to the immunohistochemistry and autoradiography images, to reduce formation of alienating noise artifacts. Matching ROIs were drawn over the aligned tumor sections. Only pixels containing tumor tissue were included. The GraphPad Prism software package (version 4.0a; GraphPad Software) was used to create scatterplots of coregistered pixel gray-scale values and to fit the resulting plots to a regression line.

Statistics

Statistical analyses were performed on a Macintosh computer (Apple) using GraphPad Prism (version 4.0a). Linear regression analysis was used to assess correlations between different parameters, and a P value of 0.05 or less was considered significant. Results are expressed as mean value \pm SD, unless stated otherwise.

RESULTS

Autoradiography and Immunohistochemistry

Qualitative analysis of autoradiography images of ^{111}In -cG250 at 4 h after injection showed a microscopic uptake pattern, with minimal spatial correlation to immunohistochemical CAIX staining. This relation was more distinct at 24 h after injection, with ^{111}In -cG250 uptake in the same areas as CAIX expression (Fig. 1). When qualitatively comparing the ^{89}Zr -cG250-F(ab')₂ autoradiography uptake signal with the immunohistochemically stained CAIX signal, a strikingly similar intratumoral distribution was obtained already at 4 h after injection (Fig. 2). Pixel-by-pixel analysis of the 200 × 200 μm gray-scale values of autoradiography and immunohistochemistry images yielded correlation coefficients (*r*) from 0.60 to 0.74 at 4 h after injection and from 0.57 to 0.66 at 24 h after injection (all correlations, *P* < 0.0001). Mean correlations and slopes of regression lines are summarized in Table 1.

Assessment of the immunohistochemically stained tumor sections showed CAIX expression always within boundaries of the pimonidazole signal but less extensive (Fig. 2C). Significant correlations between pimonidazole signal and ^{89}Zr -cG250-F(ab')₂ uptake signal were also obtained, with a range of *r* values from 0.46 to 0.68 (all correlations, *P* < 0.0001; Table 1). No correlation was found between

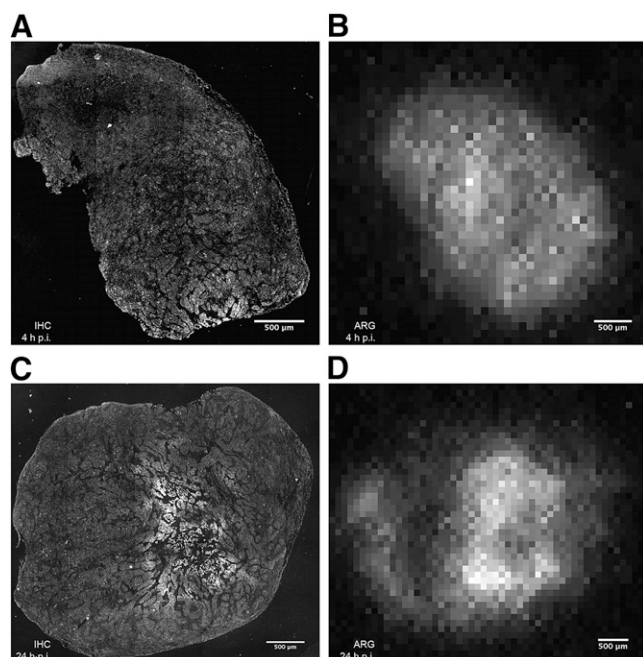


FIGURE 1. Gray-scale images of tumor sections immunohistochemically stained for CAIX (A and C) and autoradiograms of ^{111}In -cG250 (B and D) at 4 (A and B) and 24 h (C and D) after injection. At 4 h after injection, uptake of ^{111}In -cG250 is nonspecific and not localized in region of high CAIX expression. At 24 h after injection, more distinct correlation is present. ARG = autoradiography; IHC = immunohistochemistry; p.i. = after injection.

^{89}Zr -cG250-F(ab')₂ and the perfusion marker Hoechst 33342 (mean *r*, -0.01 ± 0.07 at 4 h after injection and -0.06 ± 0.08 at 24 h after injection; all correlations, *P* < 0.0001) or vascular parameters (Fig. 3).

Small-Animal PET

PET scans in 8 mice showed accumulation of ^{89}Zr -cG250-F(ab')₂ in the tumors at both 4 and 24 h after injection (Fig. 4). Mean SUV_{max} for tumors was 1.65 ± 0.26 (*n* = 4) at 4 h after injection and 0.57 ± 0.32 (*n* = 2) at 24 h after injection. The corresponding SUV_{max} in muscle tissue was 0.38 ± 0.05 and 0.14 ± 0.00 , respectively. Relatively high uptake of ^{89}Zr -cG250-F(ab')₂ was found in the kidneys (mean SUV_{max}, 12.34 ± 1.38 at 4 h after injection and 10.53 ± 0.45 at 24 h after injection) and liver (mean SUV_{max}, 2.26 ± 0.13 at 4 h after injection and 1.69 ± 0.15 at 24 h after injection). At 4 h after injection, as opposed to 24 h after injection, the heart was clearly visible on PET images, suggesting that it was actually the cardiac blood pool rather than the myocardium that was visualized at 4 h after injection (data not shown).

Tumor-to-Nontumor Ratios

Mean tumor uptake of ^{89}Zr -cG250-F(ab')₂, as determined by counting dissected tissues, was 3.71 ± 0.97 %ID/g (*n* = 5) at 4 h after injection and 1.66 ± 0.48 %ID/g (*n* = 5) at 24 h after injection (Fig. 5). Tumor uptake of ^{89}Zr -cG250-F(ab')₂ correlated well with SUV_{max} as determined from PET images (*r* = 0.93, *P* = 0.0067; Fig. 5B).

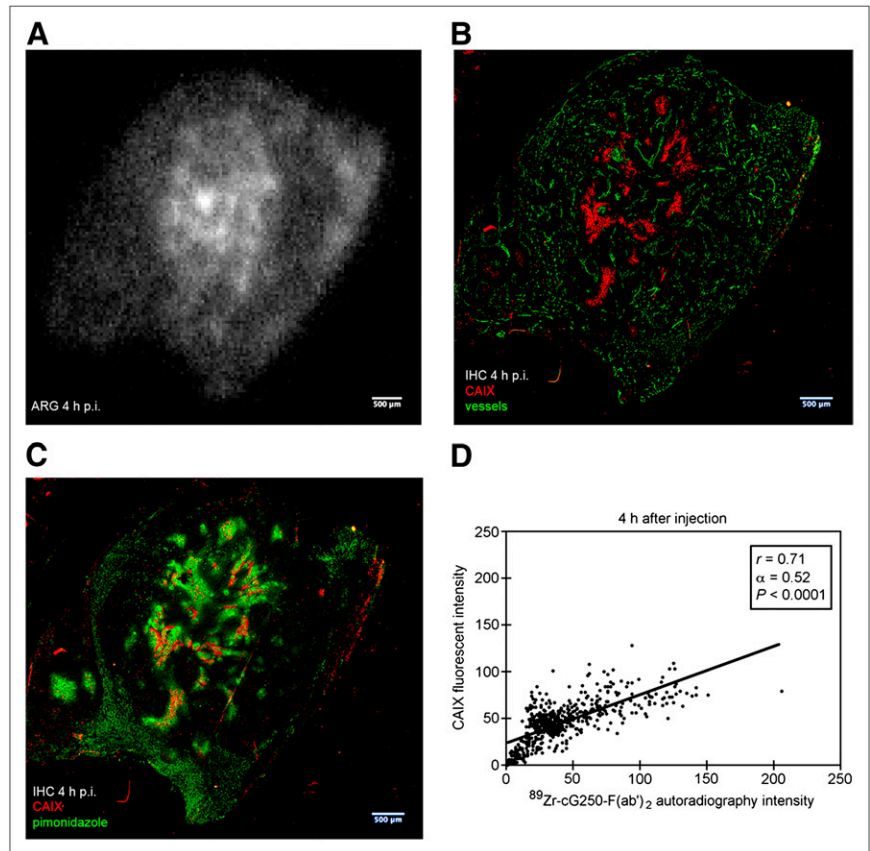
Mean concentration of ^{89}Zr -cG250-F(ab')₂ in the blood decreased from 4.34 ± 0.27 %ID/g (*n* = 5) at 4 h after injection to 0.20 ± 0.06 %ID/g (*n* = 5) at 24 h after injection. Consequently, the mean tumor-to-blood ratio increased from 0.86 ± 0.26 at 4 h after injection to 8.72 ± 3.45 at 24 h after injection. The mean tumor-to-muscle ratio was 6.83 ± 1.95 (*n* = 5) at 4 h after injection and 7.47 ± 2.45 (*n* = 5) at 24 h after injection.

^{89}Zr -cG250-F(ab')₂ Tumor Uptake and Hypoxia

Absolute tumor uptake of ^{89}Zr -cG250-F(ab')₂ and overall expression of CAIX were low. In tumor sections, the mean fraction of CAIX was 0.01 ± 0.006 . There was a significant positive correlation between fCAIX in tumor sections and uptake of ^{89}Zr -cG250-F(ab')₂ as determined by biodistribution (*r* = 0.75, *P* = 0.03; Supplemental Fig. 2A). The mean fPIMO (0.11 ± 0.05) was 10-fold higher than the mean fCAIX in tumor sections. A significant correlation between fPIMO and tumor ^{89}Zr -cG250-F(ab')₂ uptake was also found (*r* = 0.78, *P* = 0.02; Supplemental Fig. 2B). There was only a moderate and nonsignificant correlation between fCAIX and fPIMO (*r* = 0.49, *P* = 0.21).

DISCUSSION

The aim of the present study was to demonstrate the feasibility of using ^{89}Zr -cG250-F(ab')₂ as a hypoxia-related



PET marker in a human head and neck xenograft tumor model. The first experiment showed spatial correlation between ^{111}In -cG250 IgG uptake in SCCNij3 tumors and CAIX staining in tumor sections only at 24 h after injection. Nonspecific staining patterns early after injection are likely a result of diffusion- and perfusion-related characteristics of the radiotracer and tumor model. The large IgG molecules diffuse relatively slowly into the tumor tissue. As early as 4 h after injection of ^{89}Zr -cG250-F(ab')₂, efficient tumor accumulation in regions with CAIX expression was observed in SCCNij3 tumors. This specific accumulation was also present at 24 h after injection, albeit that tumor uptake and, consequently, SUV_{max} were lower.

In several studies, immunohistochemical comparison between staining for CAIX and various hypoxia-related markers showed some degree of microscopic overlap (23,24). However, colocalization analyses of exogenous markers such as pimonidazole and endogenous markers such as CAIX have yielded conflicting results (14,25). Mismatches between the spatial distribution of these 2 classes of hypoxia markers may be related to the different oxygen levels at which they are trapped, bio-reduced, or expressed, respectively; local temporal fluctuations in the level of hypoxia (i.e., acute vs. chronic hypoxia); and nonhypoxia-related factors that affect CAIX expression (26). Molecular size-related kinetic

TABLE 1. Spatial Correlation Between ^{89}Zr -cG250-F(ab')₂ Autoradiography and Immunohistochemical Signal of CAIX and Pimonidazole

Time after injection of ^{89}Zr -cG250-F(ab') ₂ (h)	^{89}Zr -cG250-F(ab') ₂ vs. CAIX		^{89}Zr -cG250-F(ab') ₂ vs. pimonidazole	
	Mean correlation coefficient (<i>r</i>)	Mean slope (α)	Mean correlation coefficient (<i>r</i>)	Mean slope (α)
4 (<i>n</i> = 4)	0.68 ± 0.06	0.31 ± 0.15	0.54 ± 0.08	0.25 ± 0.07
24 (<i>n</i> = 4)	0.62 ± 0.04	0.36 ± 0.28	0.61 ± 0.09	0.38 ± 0.11
All (<i>n</i> = 8)	0.65 ± 0.05	0.33 ± 0.21	0.58 ± 0.09	0.31 ± 0.11

Data are given as mean ± SD. Correlation coefficients (*r*) and mean linear regression slopes (α) result from 200 × 200 μm pixel-by-pixel comparison between ^{89}Zr -cG250-F(ab')₂ autoradiography images and immunohistochemical signal images of CAIX and pimonidazole.

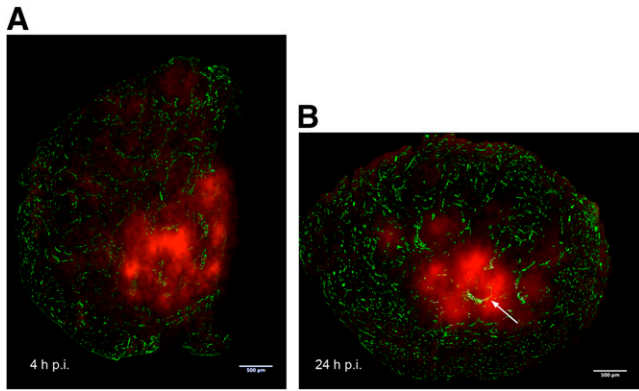


FIGURE 3. Disparity between vessels (green) and localization of high ^{89}Zr -cG250-F(ab')₂ signal (red) in tumor sections at 4 (A) and 24 h (B) after injection. As early as 4 h after injection, ^{89}Zr -cG250-F(ab')₂ binding in tumor was not perfusion-dependent. Central vessel in B (arrow) was not perfused (absence of Hoechst 33342 staining; for clarity Hoechst signal is not shown). p.i. = after injection.

characteristics of exogenous probes can also be confounding factors.

Increased expression of CAIX was found to be related to poor prognosis in several tumor types, both as an independent factor and in correlation with other markers of hypoxia (27,28).

Previously, we showed that the half-life of hypoxic cell turnover in the SCCNij3 tumor line was approximately 49 h (29). This implies that the hypoxic population remained fairly stable between injection of ^{89}Zr -cG250-F(ab')₂ and immunohistochemical staining of the CAIX and pimonida-

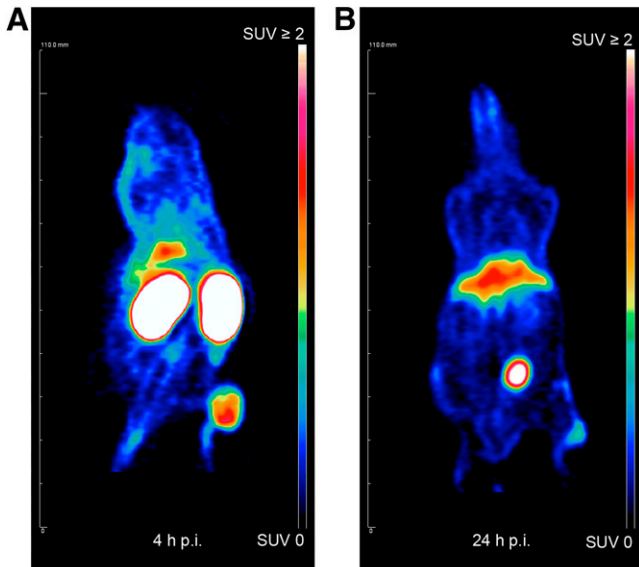


FIGURE 4. PET images of mice with tumor located subcutaneously on right hind leg at 4 (A) and 24 h (B) after injection. p.i. = after injection; SUV = standardized uptake value.

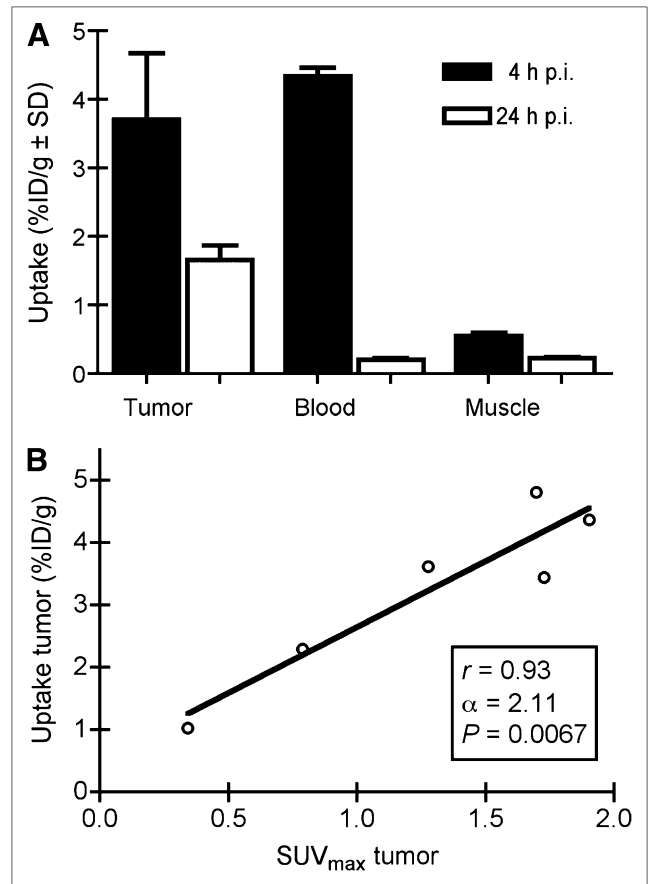


FIGURE 5. Biodistribution of ^{89}Zr -cG250-F(ab')₂ in tumor, blood, and muscle at 4 and 24 h after injection (A). Tumor uptake of ^{89}Zr -cG250-F(ab')₂ in biodistribution measurements vs. SUV_{max} of tumor on PET scan (B). p.i. = after injection.

zole signal in the present study. Fluctuating or acute hypoxia may confound the outcome of CAIX quantification as an indicator of hypoxia. In the studied model, the amount of acute hypoxia is limited, which was previously shown by good correlations between fiberoptic pO₂ measurements, indicating acute plus chronic hypoxia and pimonidazole-detected chronic hypoxia (30).

Early visualization of radiolabeled cG250-F(ab')₂ is not due to perfusion artifacts, as may be the case with early imaging using ^{111}In -cG250 IgG or, for instance, ^{64}Cu (II)-diacetyl-bis(*N*⁴-methylthiosemicarbazone) (31). Absolute expression of CAIX fluorescent signal was low in these SCCNij3 xenograft tumors, consistent with a previous study (14). In that study, fCAIX and fPIMO on immunohistochemistry were not related to uptake of ^{111}In -diethylenetriaminepentaacetic acid-cG250 IgG as determined by biodistribution measurements. Uptake of whole antibody was much higher (25.2 ± 6.2 %ID/g), as compared with uptake of ^{89}Zr -cG250-F(ab')₂ in our study (2.68 ± 1.30 %ID/g). Tumor uptake of intact IgG is usually higher than that of its fragmented form (32,33). This is due to the much

longer circulatory half-life of IgG, because high blood levels are the driving force for tumor accumulation. Compared with ^{131}I -cG250 in a mouse model with subcutaneous SK-RC-52 human renal cell carcinoma xenografts, ^{125}I -cG250-F(ab')₂ fragments cleared more quickly from the blood and normal tissues, and absolute uptake in tumor and normal tissues was considerably lower (17). Maximum tumor uptake of cG250-F(ab')₂ was reached at the earliest measuring time 1 d after injection, compared with 3 d after injection for radiolabeled intact cG250. In renal cell cancer patients, ^{131}I -cG250-F(ab')₂ cleared faster from the body than did intact IgG, whereas uptake of radioiodinated F(ab')₂ fragments in renal cell carcinoma did not exceed that of normal kidney tissue and could hardly be quantified on images. van Dijk et al. registered a higher uptake of ^{125}I -labeled G250-F(ab')₂ at 6 h after injection than at later times in a human renal cell carcinoma xenograft model (32). This decline in uptake within several hours after a relatively fast peak uptake is in line with our observations. These findings suggest the possibility of labeling cG250-F(ab')₂ with radionuclides that have a shorter half-life—such as ^{18}F and ^{64}Cu —for imaging.

There was a strong positive correlation between SUV_{max} on PET images and measured tumor uptake of ^{89}Zr -cG250-F(ab')₂ (%ID/g) in the current study. A similar correlation was found for SUV_{max} and tumor uptake of ^{124}I -cG250 in the SK-RC-52 xenograft model (34). In these tumors, a 10-fold higher SUV_{max} was reached, compared with our measurements of ^{89}Zr -cG250-F(ab')₂ uptake in a head and neck carcinoma model. However, peak measurements were not reached until 48 h after injection and blood clearance was complete at 7 d after injection—a disadvantage with respect to hypoxia imaging. The differences may be explained by the use of whole IgG versus F(ab')₂ and the homogeneous and higher levels of CAIX expression in the RCC tumor model versus the inhomogeneous, hypoxia-related CAIX expression in the head and neck tumor model.

When analyzing PET markers of hypoxia on a microscopic level, several groups have reported variable correlations between autoradiography signal and immunohistochemical marker signals in different tumor types. Troost et al. found only a weak correlation between ^{18}F -fluoromisonidazole autoradiography and pimonidazole signal on immunohistochemistry in untreated SCCNij3 xenograft tumors, using pixel-by-pixel analysis (35). Our findings are similar to results of other studies, reporting significant positive correlations between nitroimidazole derivatives and hypoxic PET tracers ^{18}F -fluoroazomycin arabinoside and ^{64}Cu (II)-diacetyl-bis(*N*⁴-methylthiosemicarbazone) at the microscopic level in different tumor models (36–38). The advantage of radiolabeled cG250-F(ab')₂, as compared with these tracers, would be that it specifically targets viable tumor cell populations that have upregulated intrinsic mechanisms to survive and adapt to a hypoxic microenvironment. These are likely the same resistant populations that are important for radiotherapy outcome. Further studies

are warranted to verify the value of radiolabeled cG250-F(ab')₂ as a hypoxia tracer against established hypoxia tracers. Recently, a simplified method to label antibodies with ^{89}Zr has been described, which will allow broader application of this radionuclide in immuno-PET studies (39).

The kidneys and liver exhibited high uptake of ^{89}Zr -cG250-F(ab')₂ by PET. In several studies, uptake of F(ab')₂ antibody fragments in murine kidneys has been reported to be higher than that of intact antibodies (15,33). A high uptake of F(ab')₂ in the kidneys likely results from fragment reabsorption by the renal tubular cells. High renal uptake could in the clinical situation interfere with imaging of tumor deposits near the kidneys.

cG250-F(ab')₂ could prove to be a useful tool in defining CAIX-positive hypoxic areas requiring intensified therapy in primary head and neck carcinomas, for instance, through redistribution of radiation dose. Additionally, CAIX-targeting inhibitors such as sulfonamides offer promising modalities in anticancer therapy (40). Clinical application of these agents will require a noninvasive imaging tool for the quantification and monitoring of CAIX expression, which could possibly be provided by cG250-F(ab')₂.

CONCLUSION

We have established a significant spatial correlation between binding of ^{89}Zr -cG250-F(ab')₂ and expression of CAIX at the microscopic level, suggesting sufficient tumor penetration and accurate microscopic hypoxia localization of the compound. These characteristics suggest a potential role of ^{89}Zr -cG250-F(ab')₂ for noninvasive hypoxia imaging of the endogenous hypoxia-related marker CAIX in head and neck carcinomas. Further studies on this concept are warranted.

ACKNOWLEDGMENTS

We thank the central animal research facility staff for technical assistance and Peter Laverman, Wenny Peeters, Annemarie Eek, Hans Peters, and Jonathan Disselhorst for their contribution to the collection and processing of data (Radboud University Medical Centre). We thank Maria Vosjan (VU University Medical Center) for technical support.

REFERENCES

1. Hockel M, Vaupel P. Tumor hypoxia: definitions and current clinical, biologic, and molecular aspects. *J Natl Cancer Inst.* 2001;93:266–276.
2. Rademakers SE, Span PN, Kaanders JH, Sweep FC, van der Kogel AJ, Bussink J. Molecular aspects of tumour hypoxia. *Mol Oncol.* 2008;2:41–53.
3. Opavsky R, Pastorekova S, Zelnik V, et al. Human MN/CA9 gene, a novel member of the carbonic anhydrase family: structure and exon to protein domain relationships. *Genomics.* 1996;33:480–487.
4. Pastorekova S, Parkkila S, Zavada J. Tumor-associated carbonic anhydrases and their clinical significance. *Adv Clin Chem.* 2006;42:167–216.
5. Gatenby RA, Gawlinski ET. A reaction-diffusion model of cancer invasion. *Cancer Res.* 1996;56:5745–5753.

6. Wykoff CC, Beasley NJ, Watson PH, et al. Hypoxia-inducible expression of tumor-associated carbonic anhydrases. *Cancer Res.* 2000;60:7075–7083.
7. Oosterwijk E, Ruiters DJ, Hoedemaeker PJ, et al. Monoclonal antibody G250 recognizes a determinant present in renal cell carcinoma and absent from normal kidney. *Int J Cancer.* 1986;38:489–494.
8. Ahlskog JK, Schliemann C, Marlind J, et al. Human monoclonal antibodies targeting carbonic anhydrase IX for the molecular imaging of hypoxic regions in solid tumours. *Br J Cancer.* 2009;101:645–657.
9. Grabmaier K, Vissers JL, De Weijert MC, et al. Molecular cloning and immunogenicity of renal cell carcinoma-associated antigen G250. *Int J Cancer.* 2000;85:865–870.
10. Divgi CR, Pandit-Taskar N, Jungbluth AA, et al. Preoperative characterisation of clear-cell renal carcinoma using iodine-124-labelled antibody chimeric G250 (¹²⁴I-cG250) and PET in patients with renal masses: a phase I trial. *Lancet Oncol.* 2007;8:304–310.
11. Kaanders JH, Bussink J, van der Kogel AJ. Clinical studies of hypoxia modification in radiotherapy. *Semin Radiat Oncol.* 2004;14:233–240.
12. Bentzen SM. Theragnostic imaging for radiation oncology: dose-painting by numbers. *Lancet Oncol.* 2005;6:112–117.
13. Schmidt MM, Wittrup KD. A modeling analysis of the effects of molecular size and binding affinity on tumor targeting. *Mol Cancer Ther.* 2009;8:2861–2871.
14. Troost EG, Bussink J, Kaanders JH, et al. Comparison of different methods of CAIX quantification in relation to hypoxia in three human head and neck tumor lines. *Radiother Oncol.* 2005;76:194–199.
15. Massuger LF, Boerman OC, Corstens FH, et al. Biodistribution of iodine-125 and indium-111 labeled OV-TL 3 intact antibodies and F(ab')₂ fragments in tumor-bearing athymic mice. *Anticancer Res.* 1991;11:2051–2057.
16. Covell DG, Barbet J, Holton OD, Black CD, Parker RJ, Weinstein JN. Pharmacokinetics of monoclonal immunoglobulin G1, F(ab')₂, and Fab' in mice. *Cancer Res.* 1986;46:3969–3978.
17. Brouwers A, Mulders P, Oosterwijk E, et al. Pharmacokinetics and tumor targeting of ¹³¹I-labeled F(ab')₂ fragments of the chimeric monoclonal antibody G250: preclinical and clinical pilot studies. *Cancer Biother Radiopharm.* 2004;19:466–477.
18. Verel I, Visser GW, Boellaard R, Stigter-van Walsum M, Snow GB, van Dongen GA. ⁸⁹Zr immuno-PET: comprehensive procedures for the production of ⁸⁹Zr-labeled monoclonal antibodies. *J Nucl Med.* 2003;44:1271–1281.
19. Lindmo T, Boven E, Cuttitta F, Fedorko J, Bunn PA Jr. Determination of the immunoreactive fraction of radiolabeled monoclonal antibodies by linear extrapolation to binding at infinite antigen excess. *J Immunol Methods.* 1984;72:77–89.
20. Visser EP, Disselhorst JA, Brom M, et al. Spatial resolution and sensitivity of the Inveon small-animal PET scanner. *J Nucl Med.* 2009;50:139–147.
21. Rijken PF, Bernsen HJ, Peters JP, Hodgkiss RJ, Raleigh JA, van der Kogel AJ. Spatial relationship between hypoxia and the (perfused) vascular network in a human glioma xenograft: a quantitative multi-parameter analysis. *Int J Radiat Oncol Biol Phys.* 2000;48:571–582.
22. Thevenaz P, Ruttimann UE, Unser M. A pyramid approach to subpixel registration based on intensity. *IEEE Trans Image Process.* 1998;7:27–41.
23. Jonathan RA, Wijffels KI, Peeters W, et al. The prognostic value of endogenous hypoxia-related markers for head and neck squamous cell carcinomas treated with ARCON. *Radiother Oncol.* 2006;79:288–297.
24. Airley RE, Loncaster J, Raleigh JA, et al. GLUT-1 and CAIX as intrinsic markers of hypoxia in carcinoma of the cervix: relationship to pimonidazole binding. *Int J Cancer.* 2003;104:85–91.
25. Kaanders JH, Wijffels KI, Marres HA, et al. Pimonidazole binding and tumor vascularity predict for treatment outcome in head and neck cancer. *Cancer Res.* 2002;62:7066–7074.
26. Hoogsteen IJ, Lok J, Marres HA, et al. Hypoxia in larynx carcinomas assessed by pimonidazole binding and the value of CA-IX and vascularity as surrogate markers of hypoxia. *Eur J Cancer.* 2009;45:2906–2914.
27. Koukourakis MI, Bentzen SM, Giatromanolaki A, et al. Endogenous markers of two separate hypoxia response pathways (hypoxia inducible factor 2 alpha and carbonic anhydrase 9) are associated with radiotherapy failure in head and neck cancer patients recruited in the CHART randomized trial. *J Clin Oncol.* 2006;24:727–735.
28. Span PN, Bussink J, Manders P, Beex LV, Sweep CG. Carbonic anhydrase-9 expression levels and prognosis in human breast cancer: association with treatment outcome. *Br J Cancer.* 2003;89:271–276.
29. Ljungkvist AS, Bussink J, Kaanders JH, et al. Hypoxic cell turnover in different solid tumor lines. *Int J Radiat Oncol Biol Phys.* 2005;62:1157–1168.
30. Bussink J, Kaanders JH, Strik AM, Vojnovic B, van der Kogel AJ. Optical sensor-based oxygen tension measurements correlated with hypoxia marker binding in three human tumor xenograft lines. *Radiat Res.* 2000;154:547–555.
31. O'Donoghue JA, Zanzonico P, Pugachev A, et al. Assessment of regional tumor hypoxia using ¹⁸F-fluoromisonidazole and ⁶⁴Cu(II)-diacetyl-bis(N⁴-methylthiosemicarbazone) positron emission tomography: comparative study featuring microPET imaging, Po₂ probe measurement, autoradiography, and fluorescent microscopy in the R3327-AT and FaDu rat tumor models. *Int J Radiat Oncol Biol Phys.* 2005;61:1493–1502.
32. van Dijk J, Zegveld ST, Fleuren GJ, Warnaar SO. Localization of monoclonal antibody G250 and bispecific monoclonal antibody CD3/G250 in human renal-cell carcinoma xenografts: relative effects of size and affinity. *Int J Cancer.* 1991;48:738–743.
33. Khawli LA, Alauddin MM, Hu P, Epstein AL. Tumor targeting properties of indium-111 labeled genetically engineered Fab' and F(ab')₂ constructs of chimeric tumor necrosis treatment (chTNT)-3 antibody. *Cancer Biother Radiopharm.* 2003;18:931–940.
34. Lawrentschuk N, Lee FT, Jones G, et al. Investigation of hypoxia and carbonic anhydrase IX expression in a renal cell carcinoma xenograft model with oxygen tension measurements and ¹²⁴I-cG250 PET/CT. *Urol Oncol.* June 11, 2009 [Epub ahead of print].
35. Troost EG, Laverman P, Kaanders JH, et al. Imaging hypoxia after oxygenation-modification: comparing [¹⁸F]FMISO autoradiography with pimonidazole immunohistochemistry in human xenograft tumors. *Radiother Oncol.* 2006;80:157–164.
36. Busk M, Horsman MR, Jakobsen S, et al. Imaging hypoxia in xenografted and murine tumors with ¹⁸F-fluoroazomycin arabinoside: a comparative study involving microPET, autoradiography, PO₂-polarography, and fluorescence microscopy. *Int J Radiat Oncol Biol Phys.* 2008;70:1202–1212.
37. Tanaka T, Furukawa T, Fujieda S, Kasamatsu S, Yonekura Y, Fujibayashi Y. Double-tracer autoradiography with Cu-ATSM/FDG and immunohistochemical interpretation in four different mouse implanted tumor models. *Nucl Med Biol.* 2006;33:743–750.
38. Yuan H, Schroeder T, Bowsher JE, Hedlund LW, Wong T, Dewhurst MW. Intertumoral differences in hypoxia selectivity of the PET imaging agent ⁶⁴Cu(II)-diacetyl-bis(N⁴-methylthiosemicarbazone). *J Nucl Med.* 2006;47:989–998.
39. Perk LR, Vosjan MJ, Visser GW, et al. p-Isothiocyanatobenzyl-desferrioxamine: a new bifunctional chelate for facile radiolabeling of monoclonal antibodies with zirconium-89 for immuno-PET imaging. *Eur J Nucl Med Mol Imaging.* 2010;37:250–259.
40. Cecchi A, Hulikova A, Pastorek J, et al. Carbonic anhydrase inhibitors: design of fluorescent sulfonamides as probes of tumor-associated carbonic anhydrase IX that inhibit isozyme IX-mediated acidification of hypoxic tumors. *J Med Chem.* 2005;48:4834–4841.